molecular pharmaceutics

Article

Cite This: Mol. Pharmaceutics 2019, 16, 2106−2117

pubs.acs.org/molecularpharmaceutics

Development and Evaluation of an ^{18}F-Radiolabeled Monocyclam Derivative for Imaging CXCR4 Expression

Diana Brickute,[†] Marta Braga,[†] Maciej A. Kaliszczak, Chris Barnes, Doreen Lau, Laurence Carroll, Elizabeth Stevens, Sebastian Trousil, Israt S. Alam, Quang-Dé Nguyen, and Eric O. Aboagye*

Cancer Imaging Centre, Department of Surgery and Cancer, Faculty of Medicine, Imperial College London, Hammersmith Hospital Campus, Du Cane Road, London W12 0NN, U.K.

Supporting Information

ABSTRACT: In humans, C−X−C chemokine receptor type 4 (CXCR4) is a protein that is encoded by the *CXCR4* gene and binds the ligand CXCL12 (also known as SDF-1). The CXCR4−CXCL12 interaction in cancer elicits biological activities that result in tumor progression and has accordingly been the subject of significant investigation for detection and treatment of the disease. Peptidic antagonists have been labeled with a variety of radioisotopes for the detection of CXCR4, but the methodology utilizing small molecules has predominantly used radiometals. We report here the development of a ^{18}F-radiolabeled cyclam-based small molecule radioprobe, [^{18}F]MCFB, for imaging CXCR4 expression. The IC_{50} value of [^{19}F]MCFB for CXCR4 was similar to that of AMD3465 (111.3 and 89.8 nM, respectively). *In vitro* binding assays show that the tracer depicted a differential CXCR4 expression, which was blocked in the presence of AMD3465, demonstrating the specificity of [^{18}F]MCFB. Positron emission tomography (PET) imaging studies showed a distinct uptake of the radioprobe in lymphoma and breast cancer xenografts. High liver and kidney uptakes were seen with [^{18}F]MCFB, leading us to further examine the basis of its pharmacokinetics in relation to the tracer's cationic nature and thus the role of organic cation transporters (OCTs). Substrate competition following the intravenous injection of metformin led to a marked decrease in the urinary excretion of [^{18}F]MCFB, with moderate changes observed in other organs, including the liver. Our results suggest involvement of OCTs in the renal elimination of the tracer. In conclusion, the ^{18}F-radiolabeled monocyclam, [^{18}F]MCFB, has potential to detect tumor CXCR4 in nonhepatic tissues.

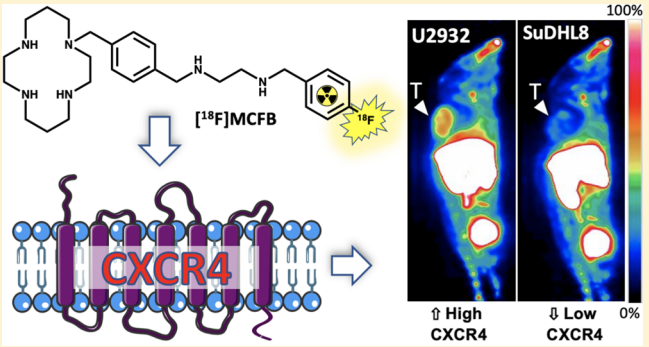

KEYWORDS: *CXCR4, cyclam, [^{18}F]MCFB, AMD3465*

INTRODUCTION

In humans, C−X−C chemokine receptor type 4 (CXCR4) is a seven-transmembrane domain G protein-coupled receptor that is encoded by the CXCR4 gene. Binding of CXCR4 to its cognate ligand, CXCL12 (also known as SDF-1), leads to the activation of several downstream signaling pathways that control cellular responses including proliferation, survival, chemotaxis, and transcription.[1,2] These CXCR4-regulated pathways exert critical functions in development and normal physiology as well as in disease processes. In fact, CXCR4 upregulation has been reported in over 20 types of malignant cancers and is correlated with poor prognosis and an aggressive phenotype. Organ-specific metastatic spread, for instance, has been attributed in part to the CXCR4−CXCL12 interaction,[3,4] wherein CXCR4-expressing tumor cells migrate to CXCL12-rich environments such as lymph nodes, lung, liver, and bone marrow. Along with the metastatic spread, the CXCR4−CXCL12 axis impacts other aspects of tumor progression, including provision of a protective niche for tumor cells in the bone marrow and supporting hypoxia-driven angiogenesis through recruitment of CXCR4-positive pro-angiogenic cells.[5,6]

Increased understanding of the pivotal role of CXCR4 in tumor biology has resulted in the development of imaging probes that can provide sensitive and rapid detection of CXCR4 expression. Positron emission tomography (PET) is a sensitive nuclear functional imaging modality used frequently in oncology for diagnosis, staging, and monitoring the treatment response. The development of novel PET imaging agents to target receptors that are characteristic of malignant phenotype is an important area of research and strives toward personalized medicine. CXCR4 is an attractive target for developing PET radioligands because of its role and overexpression in some cancers and other diseases. One of the most studied classes of CXCR4 imaging agents comprises peptidic radioprobes; screening of molecules against HIV

Received: January 15, 2019
Revised: March 14, 2019
Accepted: March 18, 2019
Published: March 18, 2019

DOI: 10.1021/acs.molpharmaceut.9b00069
Mol. Pharmaceutics 2019, 16, 2106−2117

infection led to the discovery of T140, a 14-residue peptide with a disulphide bridge that has been functionalized with various chelators/radionuclides for CXCR4 detection.[7−9] Cyclopentapeptides have also been used for the development of new imaging tracers. An important milestone in CXCR4 imaging was achieved by Demmer et al. in developing a ^{68}Ga-labeled cyclopentapeptide, [^{68}Ga]CPCR4-2 ([^{68}Ga]-Pentixafor), which has reached clinical trials because of its persistent tumor accumulation and favorable pharmacokinetics.[10,11]

An extensive array of small-molecule CXCR4 antagonists covering over 20 different chemical classes of compounds have been developed and discussed;[12] however, their application to imaging has been limited. The cyclam AMD3465 (Figure 1)

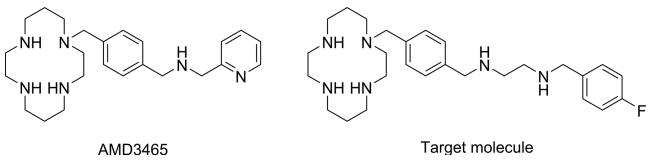

Figure 1. Chemical structures of the target molecule (MCFB or compound **5**) and AMD3465.

and bicyclam AMD3100 currently represent the most studied class of nonpeptide CXCR4 inhibitors for nuclear imaging, predominantly PET. The metal-chelating properties of cyclams have been used to radiolabel both AMD3100 and AMD3465 with ^{64}Cu.[13−16] Whereas both compounds gave a significant tumor uptake in a CXCR4-expressing transgenic cell line, [^{64}Cu]AMD3465 was more hydrophilic and showed superior pharmacokinetic properties in comparison to [^{64}Cu]-AMD3100, resulting in higher tumor imaging contrast. Both compounds, however, exhibited a considerable uptake in the liver and kidneys; the liver uptake has been hypothesized to be partly due to transchelation of ^{64}Cu to liver. Other strategies have been evaluated, whereby AMD3100 and AMD3465 were radiolabeled with ^{68}Ga[17] and ^{11}C,[18] respectively; however, these copper-free approaches showed no improvements in biodistribution in vivo. Notably, the high liver uptake,[14,18,19] independent of use of radiometal or transchelation, has been assigned in part to the previously reported cytoplasmic and cell-surface expression of the CXCR4 protein in the liver tissue.[20] Less studied is, however, the role of nonspecific transporters—in particular, organic cation transporters (OCTs), given the cationic nature of the cyclam probes—in the liver uptake of the tracers.

Despite the superior properties of the ^{18}F-radioisotope, such as low positron energy and adequate half-life (109.7 min), strategies employing this radionuclide for small-molecule labeling are limited. A few pyrimidine-based derivatives were labeled with ^{18}F. The small molecule and CXCR4 modulator, MSX-122, was shown to inhibit tumor metastasis and inflammation *in vitro*; however, no *in vivo* imaging evaluation was carried out.[21] Another pyrimidine-pyridine derivative showed no probe accumulation in CXCR4-expressing tumors because of rapid metabolism of the radioligand.[22] Work by Poty et al. used AMD3100 analogues as precursors for ^{18}F labeling, but no *in vivo* validation was performed.[23] A structurally similar tracer to AMD3465, [^{18}F]RPS-544, has been evaluated recently.[24] The radioligand showed a moderate uptake in the PC3-CXCR4 tumor model, and in addition to substantial uptake in the liver and kidneys, [^{18}F]RPS-544 also accumulated in small and large intestines, differing from the excretion profile of other labeled cyclams.

In this study, we aimed at developing and evaluating a new CXCR4-targeting radioligand that would capitalize on the advantages of ^{18}F while preserving the ability to sensitively detect CXCR4 expression in tumors. Because of the potent binding affinity and selectivity of AMD3465 toward CXCR4, this molecule was chosen as a reference for the development of the tracer, [^{18}F]MCFB.

The most important aspect of the tracer design was the high *in vivo* metabolic stability. Pyridines can generally be reacted with [^{18}F]fluoride in the 2 or 4 position to obtain the corresponding labeled fluoropyridines.[25] However, their *in vivo* stability is unpredictable, often resulting in defluorination, with an associated uptake of radioactivity in the bone.[22,24] Therefore, to facilitate ^{18}F labeling, the 2-pyridylmethylamine moiety was substituted with 1-aminomethyl-4-fluorobenzene. The former was linked to the original 1,4-phenylenebis-methylene linker by the N-substituted ethylene chain. The introduction of the ^{18}F isotope was achieved by using the easily accessible prosthetic group, [^{18}F]fluorobenzaldehyde, which can be further converted into [^{18}F]fluorobenzylamine through reductive amination.[26]

The applicability of [^{18}F]MCFB for sensitive and specific imaging of CXCR4 was evaluated as well as its *in vivo* pharmacokinetics and biodistribution in relevant tumor models.

MATERIALS AND METHODS

Materials. Unless otherwise indicated, reagents and solvents were purchased from Sigma-Aldrich (Haverhill, UK) and used without further purification. AMD3465 was purchased from Tocris Bioscience (R&D Systems, Abingdon, UK).

4-*N*,*N*,*N*-Trimethylammonium benzaldehyde (triflate salt) was synthesized according to a method published in the literature.[27] Flash column chromatography was carried out on silica gel (Aldrich silica gel, pore size 60 Å, particle size 230−400 mesh). Thin-layer chromatography (TLC) was performed on Merck Silica 60 F_{254} plates. ^{1}H nuclear magnetic resonance (NMR), ^{13}C NMR, and ^{19}F NMR were recorded on a Bruker AV-400 spectrometer at a frequency of 400, 101, and 376 MHz, respectively. Chemical shifts (δ) are given in parts per million as referenced to the appropriate residual solvent peaks. Signals are assigned as s, d, m, and br for singlet, doublet, multiplet, and broad, respectively. ^{13}C NMRs are complicated by the existence of C−F coupling (long range including) and conformers. Mass spectra (m/z) were obtained in a positive electrospray ionization on a Waters LCT Premier (electrospray ionization time-of-flight mass spectrometer). Crude reaction mixtures were analyzed by TLC and high-performance liquid chromatography (HPLC).

HPLC Methods. (a) Purity analysis of nonradioactive and radioactive compounds was carried out on a Shimadzu Prominence HPLC system equipped with a LC-10Ai pump, an SPD-20A UV detector (λ = 254 nm), a Flow-RAM sodium iodide/PMT gamma detector, and Laura 4.1.1.3 software (LabLogic); Phenomenex Gemini 5μ C18 150 × 4.6 mm and Luna 5μ Phenyl-Hexyl 150 × 4.6 mm columns were used, and a mobile phase comprising water (0.1% TFA)/MeCN with a gradient of 5% organic for 1 min, 5 → 95% for 16 min, 95% organic for 2 min, and 95 → 5% organic for 2 min delivered at a flow rate of 1 mL/min. (b) Semipreparative radio-HPLC was

DOI: 10.1021/acs.molpharmaceut.9b00069
Mol. Pharmaceutics 2019, 16, 2106−2117

carried out using a Shimadzu LC-20AT pump, a Bioscan Flowcount FC3200 sodium iodide/PMT gamma detector (LabLogic), and a Knauer UV detector (λ = 254 nm). Sample injection, product isolation, and data collection were performed using an in-house built multistream HPLC system, bespoke software package (Hammersmith Imanet Ltd., UK), and an Agilent 5μ Eclipse XDB-C18 250 × 9.4 mm column with an isocratic mobile phase of water (0.1% TFA)/MeCN (62:38 v/v) at a flow rate of 3 mL/min; injection loop 10 mL. (c) Metabolite analysis was carried out using an Agilent 1100 series G1312A pump and LabLogic Laura 3 software equipped with a linear G1314A UV detector (λ = 254 nm), a γ-RAM model 3 detector, and a Phenomenex Luna 5μ Phenyl-Hexyl 250 × 10 mm column with an isocratic mobile phase of water (0.1% TFA)/MeCN (80:20 v/v) at a flow rate of 3 mL/min; injection loop 1 mL.

Synthesis of Precursor and Reference Compound. *1,1′,1″-(1,4,8,11-Tetraazacyclotetradecane-1,4,8-triyl)tris-(2,2,2-trifluoroethan-1-one) (**1**).* To a stirred solution of cyclam (1 g, 4.99 mmol) and triethylamine (TEA, 0.69 mL, 4.99 mmol) in methanol (10 mL) was added ethyl trifluoroacetate (EtOTFA, 2.36 mL, 19.9 mmol) dropwise. The homogeneous reaction mixture was cooled with an ice-water bath to control the mild exothermic reaction. Stirring was continued under N_2 overnight. Volatiles were removed under reduced pressure. The residue was dissolved in EtOAc and passed through the plug of silica. The solvent was concentrated to give the product as a white foam (2.6 g, 93%). HRMS (ESI) = 489.1549 $(M + H)^+$ calcd for $C_{16}H_{22}N_4O_3F_9$, 489.1548. ^{1}H NMR (400 MHz, $CDCl_3$): δ 3.91−3.34 (m, 12H), 3.07−2.84 (m, 2H), 2.81−2.50 (m, 2H), 2.40−2.07 (m, 2H), 1.98−1.67 (m, 2H), 1.17−0.60 (br s, 1H). ^{13}C NMR (101 MHz, $CDCl_3$): δ 160.06−154.85 (m, C═O), 121.77−111.81 (q, CF_3, J = 288.6 Hz), 52.55−43.85 (m, CH_2−N), 31.74−25.94 (m, CH_2). ^{19}F NMR (376 MHz, $CDCl_3$): δ −63.56 to −72.90 (m).

*1,1′,1″-(11-(4-(Bromomethyl)benzyl)-1,4,8,11-tetraazacyclotetradecane-1,4,8-triyl)tris(2,2,2-trifluoroethan-1-one) (**2**).* To a stirred solution of **1** (1.95 g, 3.99 mmol) and K_2CO_3 (717 mg, 5.2 mmol) in CH_3CN (70 mL) was added α,α'-dibromo-*p*-xylene (5.25 g, 19.9 mmol), and the reaction mixture was stirred at 70 °C for 1 h. The solution was cooled to room temperature, and the solvent was removed under reduced pressure. The residue was partitioned between brine (50 mL) and CH_2Cl_2 (100 mL). The organic phase was separated, dried (Na_2SO_4), and silica added, and the mixture was evaporated to dryness. The compound impregnated on silica was purified by flash chromatography (first with CH_2Cl_2, followed by CH_2Cl_2/ether, 9:1) to give the desired compound as a white solid (1.8 g, 67%). HRMS (ESI) = 671.1273 $(M + H)^+$ calcd for $C_{24}H_{29}N_4O_3BrF_9$, 671.1279. ^{1}H NMR (400 MHz, $CDCl_3$): δ 7.55−7.01 (m, 4H), 4.50 (s, 2H), 3.99−3.23 (m, 14H), 2.95−2.62 (m, 2H), 2.62−2.27 (m, 2H), 2.28−1.92 (m, 2H), 1.90−1.43 (m, 2H). ^{13}C NMR (101 MHz, $CDCl_3$): δ 158.07−156.48 (m), 138.23−136.41 (m), 130.55−128.42 (m), 120.99−111.59 (m), 61.02−58.94 (m), 56.06−44.52 (m), 33.30−32.47 (m), 29.95−23.65 (m). ^{19}F NMR (376 MHz, $CDCl_3$): δ −68.31 to −69.57 (m).

*1,1′,1″-(11-(4-(((2-Aminoethyl)amino)methyl)benzyl)-1,4,8,11-tetraazacyclotetradecane-1,4,8-triyl)tris(2,2,2-trifluoroethan-1-one) (**3**).* To a stirred solution of ethylenediamine (134 mg, 2.2 mmol) and K_2CO_3 (93 mg, 0.675 mmol) in dry CH_3CN (5 mL) at −10 °C (acetone/ice bath) was added dropwise a solution of 1-[1-methylene-4-(bromomethylene)phenylene]-4,8,11-tris(trifluoroacetyl)-1,4,8,11-tetra-azacyclotetradecane (**2**) (300 mg, 0.45 mmol) in CH_3CN (20 mL) over 15−20 min. After stirring for a further 30 min, the reaction mixture was filtered and concentrated to provide a residue, which was purified by chromatography on silica gel using 1% TEA in EtOAC/MeOH (7:3) to give the product as a white solid (180 mg, 62%). HRMS (ESI) = 651.2708 $(M + H)^+$ calcd for $C_{26}H_{36}N_6O_3F_9$, 651.2705. ^{1}H NMR (400 MHz, DMSO-d_6): δ 7.33−7.10 (m, 4H), 3.87−3.18 (m, 15H), 3.09−2.24 (m, 12H), 2.18−1.95 (m, 2H), 1.83−1.63 (m, 2H). ^{13}C NMR (101 MHz, DMSO-d_6): δ 157.30−154.95 (m), 141.15−139.76 (m), 137.61−136.04 (m), 130.23−127.12 (m), 121.54−111.81 (m), 59.71−58.30 (m), 54.43−43.32 (m), 41.65 (s), 29.51−22.06 (m). ^{19}F NMR (376 MHz, DMSO-d_6): δ −66.66 to −74.74 (m).

*1,1′,1″-(11-(4-(((2-((4-Fluorobenzyl)amino)ethyl)amino)-methyl)benzyl)-1,4,8,11-tetraazacyclotetradecane-1,4,8-triyl)tris(2,2,2-trifluoroethan-1-one) (**4**).* To a stirred solution of amine **3** (100 mg, 0.153 mmol) in dry CH_3CN (10 mL), at room temperature, were added 4-fluorobenzaldehyde (12.6 μL, 0.118 mmol) and a catalytical amount of glacial acetic acid. The resulting solution was stirred at room temperature for 1 h, and $NaBH(OAc)_3$ (75 mg, 0.354 mmol) was added. The mixture was left to stir overnight. Acetonitrile was removed under vacuum. The residue was dissolved in EtOAc, washed with saturated aqueous $NaHCO_3$, dried (Na_2SO_4), concentrated, and purified by chromatography on silica gel using 0.5% TEA in EtOAC/MeOH (8:2). The desired product was obtained as a white solid (40 mg, 34%). MS (ESI): m/z 759 $[MH^+]$. ^{1}H NMR (400 MHz, DMSO-d_6): δ 7.64−6.76 (m, 8H), 3.89−3.23 (m, 19H), 3.19−2.53 (m, 6H), 2.49−2.21 (m, 2H), 2.22−1.93 (m, 3H), 1.88−1.60 (m, 2H). ^{13}C NMR (101 MHz, DMSO-d_6): δ 162.68 (s), 160.28 (s), 158.23−154.29 (m), 140.47−139.58 (m), 138.16−135.95 (m), 130.84−127.03 (m), 121.41−111.86 (m), 115.25−115.04 (d, J = 21.1 Hz), 59.86−58.02 (m), 54.38−43.14 (m), 52.46 (s), 48.49 (s), 31.53−22.35 (m). ^{19}F NMR (376 MHz, DMSO-d_6): δ −67.85 to −68.75 (m), −116.76 (s).

*N^1-(4-((1,4,8,11-Tetraazacyclotetradecan-1-yl)methyl)-benzyl)-N^2-(4-fluorobenzyl)ethane-1,2-diamine (**5**).* To a stirred solution of the trifluoroacetyl-protected amine **4** (70 mg, 0.09 mmol) in MeOH (2.0 mL), 5 N NaOH (200 μL) was added at room temperature. The resulting solution was stirred at room temperature overnight. The solvent was removed under reduced pressure, and CH_2Cl_2 (5 mL) and water (2.0 mL) were added to the residue. The phases were separated, and the aqueous phase was extracted with CH_2Cl_2 (3 × 5 mL). The combined organic phases were washed with 1 N NaOH, dried (Na_2SO_4), and concentrated to give a free base (40 mg, 93%). HRMS (ESI) = 471.3609 $(M + H)^+$ calcd for $C_{27}H_{44}N_6F$, 471.3611. ^{1}H NMR (400 MHz, $CDCl_3$): δ 7.31−7.05 (m, 6H), 7.04−6.82 (m, 2H), 3.67 (s, 4H), 3.48 (s, 2H), 2.85−2.31 (m, 23H), 1.87−1.70 (m, 2H), 1.67−1.51 (m, 2H). ^{13}C NMR (101 MHz, $CDCl_3$): δ 163.07 (s), 160.64 (s), 139.04 (s), 137.47 (s), 136.23 (d, J = 3.2 Hz), 129.62−127.86 (m), 115.34−114.84 (d, J = 21.2 Hz), 57.45 (s), 54.53 (s), 53.67 (s), 53.27 (s), 53.19 (s), 50.83 (s), 49.36 (s), 49.17 (s), 48.97 (s), 48.78 (s), 48.02 (s), 47.41 (s), 28.66 (s), 26.25 (s). ^{19}F NMR (376 MHz, $CDCl_3$): δ −116.25 (s).

Radiosynthesis of [^{18}F]MCFB. The no-carrier-added aqueous [^{18}F]fluoride solution, typically 1.5 mL, 1.4 GBq, was transferred to a FASTlab automated synthesis module (GE

DOI: 10.1021/acs.molpharmaceut.9b00069
Mol. Pharmaceutics 2019, 16, 2106−2117

Healthcare Life Sciences, Amersham, UK). The activity was trapped on a Waters QMA-carbonate Sep-Pak SPE cartridge and eluted into a reaction vessel with 1000 μL of an eluent solution [800 μL of Kryptofix 2.2.2 (6 mg/mL in acetonitrile) and 200 μL of $KHCO_3$ (3.5 mg/mL in H_2O)]. The eluate was evaporated to dryness by a combination of vacuum and nitrogen flow at 120 °C for 12 min. After drying, anhydrous acetonitrile (400 μL) was added to the dried residue in the reaction vessel, and the remaining radiosynthesis was carried out manually.

To a Wheaton vial containing 2.0 mg of 4-trimethylammonium-benzaldehyde trifluoromethanesulfonate precursor dissolved in acetonitrile (100 μL), dried [^{18}F]fluoride (370−555 MBq in 300 μL acetonitrile) was added at an ambient temperature. The labeling reaction was conducted at 90 °C for 15 min before allowing it to reach room temperature. A solution of cyclam-amine (6.0 mg) in acetonitrile (100 μL) was then added, followed by heating at 50 °C for 15 min. Afterward, the reaction mixture was cooled again to an ambient temperature, and neat sodium triacetoxyborohydride (4.5 mg) was added and heating resumed for 30 min at 50 °C. The reaction was quenched by the addition of 0.1% trifluoroacetic acid (TFA) in water (10 mL) and purified by semipreparative radio-HPLC. The fraction of eluent containing [^{18}F]-**4** was collected and diluted to a final volume of 40 mL with water and then immobilized on a Sep Pak tC18 light cartridge (Waters) [preconditioned with acetonitrile (5 mL) and water (10 mL)]. The cartridge was then washed with water (5 mL), followed by elution of the radioligand using ethanol (300 μL). To a solution of ethanol was added 1 M NaOH (200 μL), and the mixture was left at room temperature for 15 min. Formulation was achieved by the addition of 1 M HCl to provide [^{18}F]MCFB.

Radiochemical purity was confirmed by coelution with a reference compound (Supporting Information Figure S1).

log *D* Determination. Briefly, 7 MBq of the ligand in 20 μL of phosphate-buffered saline (PBS) was added to a mixture of 2 mL of *n*-octanol and 2 mL of PBS, pH 7.4; *n*-octanol was washed with PBS before use. The mixture was vigorously shaken for 1 h at room temperature and then centrifuged at 5000 rpm for 5 min; 100 μL aliquots from each of the two phases were drawn, and their radioactivity content was measured in a γ-counter (LKB Wallac 1282 Compugamma laboratory gamma counter, PerkinElmer, Massachusetts, USA). The *n*-octanol/PBS partition coefficient was determined by dividing the radioactivity found in the *n*-octanol layer by that found in the PBS layer. The log $D_{octanol/PBS}$ value is reported as the average of three independent experiments.

Cell Culture. The human triple-negative metastatic breast cancer cell lines MDA-MB-231-luc, MDA-MB-231 shSC, and MDA-MB-231 shCXCR4, the CXCR4-overexpressing glioma cell line, U87.CD4.CXCR4, and the diffuse large B-cell lymphoma cell lines, U2932 and SuDHL8, were cultured in Roswell Park Memorial Institute medium (Sigma-Aldrich). MDA-MB-231-luc (hitherto referred to as MDA-MB-231) is a luciferase-expressing wild-type MDA-MB-231 cell line obtained from PerkinElmer (Waltham, MA, USA). CXCR4 expression was silenced by doxycycline-inducible shRNA targeting CXCR4 (pTRIPZ CXCR4 shRNA clone V3THS_346208; Dharmacon, Lafayette, USA) to obtain MDA-MB-231 shCXCR4 or nontargeting shRNA (Dharmacon) to obtain MDA-MB-231 shSC. Viruses were packaged using the Trans-Lentiviral shRNA Packaging System (Dharmacon). Stable clones were FACS-sorted based on the expression of a doxycycline-inducible TurboRFP reporter gene within the same construct. CXCR4 knockdown was induced by incubation with doxycycline-hyclate (Sigma-Aldrich) for indicated times. All cell lines were cultured in the presence of 10% fetal bovine serum (Sigma-Aldrich), 2 mM L-glutamine (Invitrogen, Carlsbad, USA), and 100 U/mL penicillin-streptomycin (Invitrogen) in a humidified atmosphere of 5% CO_2 at 37 °C.

[^{125}I]SDF-1 Ligand-Binding Assay. The [^{125}I]SDF-1 ligand binding to CXCR4 on U87.CD4.CXCR4 cells and antagonism by [^{19}F]MCFB were conducted as previously described by us.[28] AMD3465 was used as the positive control.

***In Vitro* Radioligand Uptake.** Cells were seeded in six-well plates at a density of 400 000−600 000 cells/well 24 h prior to the experiment. For blocking studies, U2932 and SuDHL8 cells were treated with vehicle or 500 μg/mL AMD3465 for 5 min before the addition of radioactive compounds. For knockdown studies, MDA-MB-231 shCXCR4 or relevant shSC control cells were treated with doxycycline at a concentration of 0.5 μg/mL for 24 h prior to uptake studies. In hypoxia studies, the cells were placed within a filtered hypoxia chamber (Oxoid Anaerojar, Thermo Fisher Scientific) that achieves <1% O_2 and incubated at 37 °C, 5% CO_2 (balance N_2) for 16 h. Cells evaluated under normoxic conditions were incubated in 21% O_2, 5% CO_2, and balance N_2 for 16 h at 37 °C.

The cells were then incubated with the radioligand at 0.74 MBq/well for 60 min at 37 °C under 5% CO_2. Following incubation, the cells were placed on ice and washed three times with ice-cold PBS. After washing, the cells were lysed with RIPA buffer (Sigma-Aldrich) for 5 min. The radioactivity of the lysate was measured by γ-counting. Counts/min data were expressed as a percentage of the incubated dose (ID) of radioactivity in each well and the total cellular protein concentration of the sample, determined using the Pierce BCA assay (Thermo Fisher Scientific), that is, % ID/mg protein.

***In Vitro* Internalization Studies.** For internalization experiments, MDA-MB-231 cells were plated in six-well plates at a density of 600 000 cells/well and allowed to recover for 24 h at 5% CO_2 at 37 °C. On the day of the assay, the cells were incubated with approximately 0.74 MBq/well of [^{18}F]MCFB for 30 min at 4 °C (assuming inhibition of receptor internalization at this temperature) or at 37 °C. Under conditions incubated at 4 °C, the media was replaced with fresh 37 °C media and incubated for 5, 15, 30, and 60 min at 37 °C. After incubation, surface-bound radioactivity was removed by washing the cells with 400 μL of ice-cold 50 mM glycine in 150 mM NaCl (pH 3) for 5 min on ice, followed by two washes with ice-cold PBS. To obtain the internalized fraction, the cells were lysed with 400 μL of 1 M NaOH. The radioactivity of the internalized fraction was measured by γ-counting. Counts/min data were expressed as a percentage of the ID of radioactivity in each well and the total cellular protein concentration of the sample, determined using the Pierce BCA assay, that is, % ID/mg protein. The percentage of internalization was calculated as

$$\text{Internalization (\%)} = \frac{\text{internalized fraction}}{\text{surface bound fraction} + \text{internalized fraction}} \times 100$$

DOI: 10.1021/acs.molpharmaceut.9b00069
Mol. Pharmaceutics 2019, 16, 2106−2117

Immunoblotting. For the western blot analysis, the cells (80−90% confluency) were placed on ice, the medium was removed, and the cells were washed three times with ice-cold PBS and lysed with RIPA buffer supplemented with 100× Pierce protease and phosphatase inhibitor cocktail (Thermo Fisher Scientific) for 10 min on ice. The whole lysates were sonicated, and the total protein concentration was quantified using the Pierce BCA protein assay kit (Thermo Fisher Scientific). The lysates were mixed with NuPage LDS loading buffer and a reducing agent (Invitrogen) and denatured at 70 °C for 10 min. Equal amounts of protein (30 μg) were resolved on 4−15% Mini-PROTEAN TGX gels (Bio-Rad, Hemel Hempstead, UK) and separated by gel electrophoresis at 290 V for 15 min. The gels were then transferred to poly(vinylidene difluoride) membranes (Trans-Blot Turbo Transfer Packs, Bio-Rad) using the Trans-Blot Turbo System (Bio-Rad). Membranes were blocked for 1 h in 5% milk in PBS containing 0.1% v/v Tween 20 (Sigma-Aldrich) (PBST) and incubated with rabbit anti-human CXCR4 clone UMB2 (1:1000; ab124824, Abcam, Danvers, USA) and mouse anti-HIF-1α clone 54 (1:1000; BD Biosciences, USA) overnight at 4 °C. After washing with PBST, goat anti-rabbit immunoglobin G (IgG) horseradish peroxidase (IgG-HRP) (1:2000, SC-2004, Santa Cruz Biotechnology, Dallas, USA) or goat anti-mouse IgG-HRP (1:2000, SC-2005, Santa Cruz Biotechnology) was incubated in 5% milk-PBST for 1 h at room temperature. Signals were detected using Amersham enhanced chemiluminescence Plus Western Blotting Detection Reagent kit (GE Healthcare Life Sciences) and Amersham Hyper-film (GE Healthcare Life Sciences). The intensity of the protein bands was normalized to β-actin [mouse anti-β-actin antibody (1:10 000, ab6276, Abcam)] and analyzed using ImageJ version 1.44h (National Institutes of Health).

Immunofluorescence. For immunofluorescence staining of the tumor CXCR4 expression, formalin-fixed paraffin-embedded tumor slices (5 μm thickness) were stained with rabbit anti-CXCR4 UMB2 clone antibody (1:200) in a blocking buffer overnight at 4 °C. The slides were subsequently washed with PBST thrice and incubated with Alexa Fluor 488 goat anti-rabbit IgG secondary antibody (1:400; Molecular Probes, Thermo Fisher Scientific) in a blocking buffer for 1 h at room temperature and protected from light. Following another washing step, the slides were mounted using ProLong gold antifade reagent with 4′-6-diamidino-2-phenylindole (DAPI) (Life Technologies Ltd., Thermo Fisher Scientific). Immunofluorescence imaging was performed using a 40× or 60× UPlanAPO objective lens on an Olympus BX-51 wide-field microscopy UIS2 optical system (Olympus Life Science Europa GMBH, Hamburg, Germany) equipped with a DP70 digital camera. Images were acquired using an Olympus U-RFL-T epifluorescence source and DPController 1.2.1.108 imaging software (Olympus Optical Co. Ltd, Tokyo, Japan) in the red, blue, and green channels. Image processing was performed using ImageJ version 1.44h.

***In Vivo* Radioligand Uptake.** All animal experiments were done by licensed investigators in accordance with the UK Home Office Guidance on the Operation of the Animal (Scientific Procedures) Act 1986 (HMSO, London, UK, 1990) and within guidelines set out by the UK National Cancer Research Institute Committee on Welfare of Animals in Cancer Research.[29]

The *in vivo* models were established in female athymic nude mice (MDA-MB-231 tumor model) or in NOD/SCID mice (U2932 and SuDHL8 tumor models) aged 6 to 8 weeks (Harlan, Bicester, UK Ltd). Xenografts were established under 2.5% isoflurane anesthesia by subcutaneous injection of the MDA-MB-231 cell line (5×10^6 cells in 100 μL PBS) or U2932 and SuDHL8 [5×10^6 cells in 100 μL of 50% PBS and 50% Matrigel (Corning, Amsterdam, The Netherlands)] in the back of the neck of the mice. Tumor dimensions were measured by a caliper, and volumes were calculated using the ellipsoid formula that is best for estimating the tumor mass: volume (mm^3) = $(\pi/6) \times a \times b \times c$, where a, b, and c represent the three orthogonal axes of the tumor. Mice were used for imaging when the tumor volume reached approximately 100 mm^3 (at approximately 4−6 weeks postinduction).

For imaging, the mice were anesthetized with 2.5% isoflurane and placed in a thermostatically controlled rig in a dedicated small animal Genisys^4 PET scanner (SOFIE Biosciences, Culver City, USA). Following injection of 0.925 MBq of [^{18}F]MCFB via the lateral tail vein cannula, PET scans were acquired in a list-mode format over either 0−60 min (dynamic scan) or 40−60 min after injection (static scan) to give decay-corrected values of radioactivity accumulation in tissues. The collected data were ordered into six (dynamic scan) or two (static scan) time frames of 600 s and reconstructed with a three-dimensional maximum likelihood estimation method. Volumes of interest (VOIs) for tumors and different organs were defined using Siemens Inveon Research Workplace software (Siemens Molecular Imaging Inc., Knoxville, USA), and the count densities (MBq/mL) of these VOIs were averaged for the time points corresponding to 40−60 min (where equilibrium was observed). Tissue radioactivity uptake values were normalized to whole-body uptake, a method used in previous publications.[30−32]

Metabolism Studies. Non-tumor-bearing mice were injected intravenously with 3.7 MBq of [^{18}F]MCFB. Plasma, urine, and liver were collected at the indicated time and were snap-frozen in liquid nitrogen for the subsequent HPLC analysis. For extraction, ice-cold CH_3CN (1.0 mL) was added to the plasma. The mixture was centrifuged (15 493×g, 4 °C, 3 min), and the resulting supernatant was evaporated to dryness under vacuum at 40 °C using a rotary evaporator. The liver samples were diced and homogenized with ice-cold CH_3CN (1.0 mL) using a Precellys 24 homogenizer prior to centrifugation. The supernatant was then decanted and evaporated to dryness. The samples were resuspended in the HPLC mobile phase (1.2 mL) and filtered through a 13 mm Pall Acrodisc syringe filter (0.2 μm), and analyzed by radio-HPLC.

Biodistribution Studies. Biodistribution studies were carried out 60 min after injection of 0.925 MBq of [^{18}F]MCFB via the lateral tail vein cannula. Tissue samples were quickly collected, and the radioactivity content was determined by γ-counting and normalized to the sample weight. Treatment with metformin hydrochloride (Sigma-Aldrich) was carried out by injection of 50 mg/kg of metformin intravenously in U2932-bearing mice 30 min prior to injection of radioactive compound. The dose of metformin selected was based on the work by Wilcock and Bailey[33] that indicates that a 50 mg/kg bolus is equivalent to the maximum recommended daily dosage in humans.

Statistics. Data are expressed as mean ± standard error of the mean (SEM). Statistical analysis was done using the unpaired two-tailed Student's t-test or two-way analysis of variance with Bonferroni correction as appropriate and defined

DOI: 10.1021/acs.molpharmaceut.9b00069
Mol. Pharmaceutics 2019, 16, 2106−2117

Scheme 1. Synthesis of Compound 5 from Cyclam

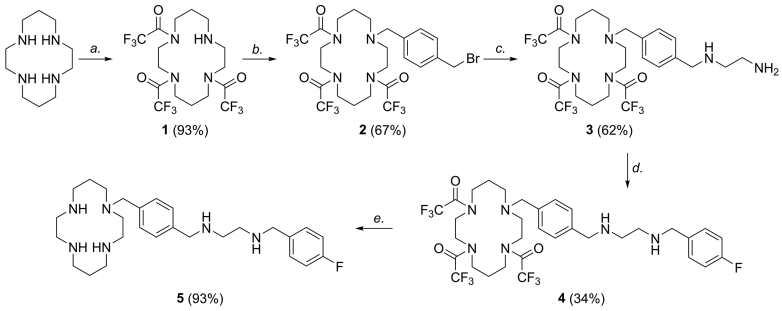

Reagents and conditions: ***a.*** ethyl trifluoroacetate, TEA, MeOH, rt; ***b.*** α,α′-dibromo-p-xylene, K_2CO_3, CH_3CN at reflux; ***c.*** ethylenediamine, K_2CO_3, CH_3CN at -10 °C; ***d.*** 4-fluorobenzaldehyde, catalytic amount of AcOH, $NaBH(OAc)_3$, CH_3CN, rt; ***e.*** 5M NaOH, MeOH, rt.

Scheme 2. Radiosynthesis of [^{18}F]MCFB. (A) Synthesis of [^{18}F]FBA. (B) Synthesis of [^{18}F]MCFB from Precursor 3 Using [^{18}F]FBA

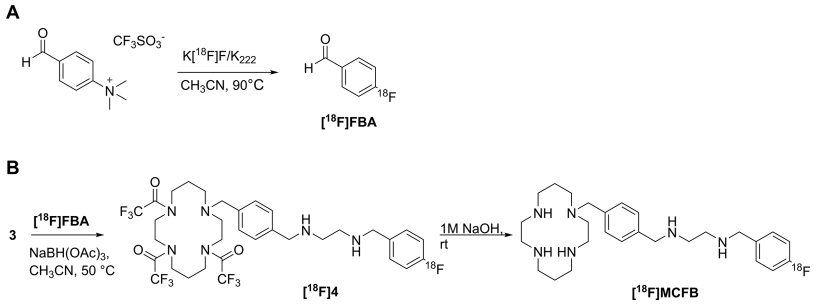

as significant (*, $0.01 < p < 0.05$), very significant (**, $0.001 < p < 0.01$), and extremely significant (***, $p < 0.001$).

RESULTS

Nonradioactive Synthesis of Precursor 3 and Reference Compound 5. The synthesis of precursor **3** and reference compound **5** is shown in Scheme 1. The protection of cyclam with EtOTFA was done using previously optimized conditions with TEA.[34] The subsequent *N*-alkylation of the triprotected cyclam **1** with α,α′-dibromo-*p*-xylene using K_2CO_3 in acetonitrile gave the desired bromomethyl intermediate **2** in 67% isolated yield. Initial attempts to alkylate ethylenediamine with intermediate **2** at an elevated temperature unfortunately increased the formation of byproducts, which were subsequently minimized by performing the reaction at −10 °C and using an excess of the diamine to give a 62% yield. Additionally, precursor **3** was further used for the preparation of reference compound **5**. First, compound **4** was prepared by the reductive amination of 4-fluorobenzaldehyde with **3** using $NaBH(OAc)_3$ in acetonitrile. Straight-forward mild deprotection of the amides via MeOH in aqueous NaOH afforded a free base within 16 h in a yield of 93%.

Radiochemistry and Partition Coefficient. The labeled variant of **5** was prepared via a three-step procedure: (a) radiosynthesis of the ^{18}F-labeling prosthetic group 4-[^{18}F]-fluorobenzaldehyde ([^{18}F]FBA) followed by (b) reductive amination and (c) global deprotection. [^{18}F]FBA was synthesized from 4-*N*,*N*,*N*-trimethylammonium benzaldehyde (triflate salt) via a standard fluorination route (K[^{18}F]F/Kryptofix 222) in acetonitrile at 90 °C for 15 min and was used for the next step without further purification (Scheme 2A). Substitution of potassium carbonate for the less basic potassium hydrogen carbonate improved the reproducibility of the reaction significantly, most likely because of the higher stability of the precursor under these conditions (as seen by the ultraviolet trace from analytical HPLC of the incorporation). The average radiochemical incorporation as measured by analytical radio-HPLC was >95%.

The subsequent step was the reductive alkylation of amine **3** with the intermediate [^{18}F]FBA using $NaBH(OAc)_3$ as the reducing agent (Scheme 2B). The reaction was performed as a one-pot two-step synthesis. Parameters such as the temperature, solvent, reaction time, and sequence of reagent addition were investigated. The optimal conditions were found to be 15 min reaction time for the initial formation of the imine (which was not isolated) and a further 30 min for subsequent reduction with $NaBH(OAc)_3$. The solvent of choice for both steps was acetonitrile, with the reaction carried out at 50 °C to produce the alkylated amine [^{18}F]**4**.

Finally, deprotection of [^{18}F]**4** was carried out using 1 M NaOH at room temperature affording the desired molecule [^{18}F]MCFB with complete conversion within 10 min. As the procedure was carried out manually with low amounts of radioactivity, only a modest specific activity (5.7 GBq/μmol) was achieved. The radiosynthetic procedure from ^{18}F fluoride including formulation of [^{18}F]MCFB took 2.5 h in total. Overall, the decay-corrected yield of 14.1 ± 2.5% (n = 5) was achieved.

The log $D_{octanol/PBS}$ of [^{18}F]MCFB was found to be −1.64 ± 0.06.

Competitive Binding, Receptor Expression, and Internalization of [^{18}F]MCFB. Binding of [^{19}F]MCFB to CXCR4 was estimated from its inhibitory effect on binding of the native ligand CXCL12 to CXCR4 in cells. [^{19}F]MCFB or AMD3465 (positive control) inhibited the CXCL12-CXCR4 interaction in a concentration-dependent manner (Supporting

DOI: 10.1021/acs.molpharmaceut.9b00069
Mol. Pharmaceutics 2019, 16, 2106−2117

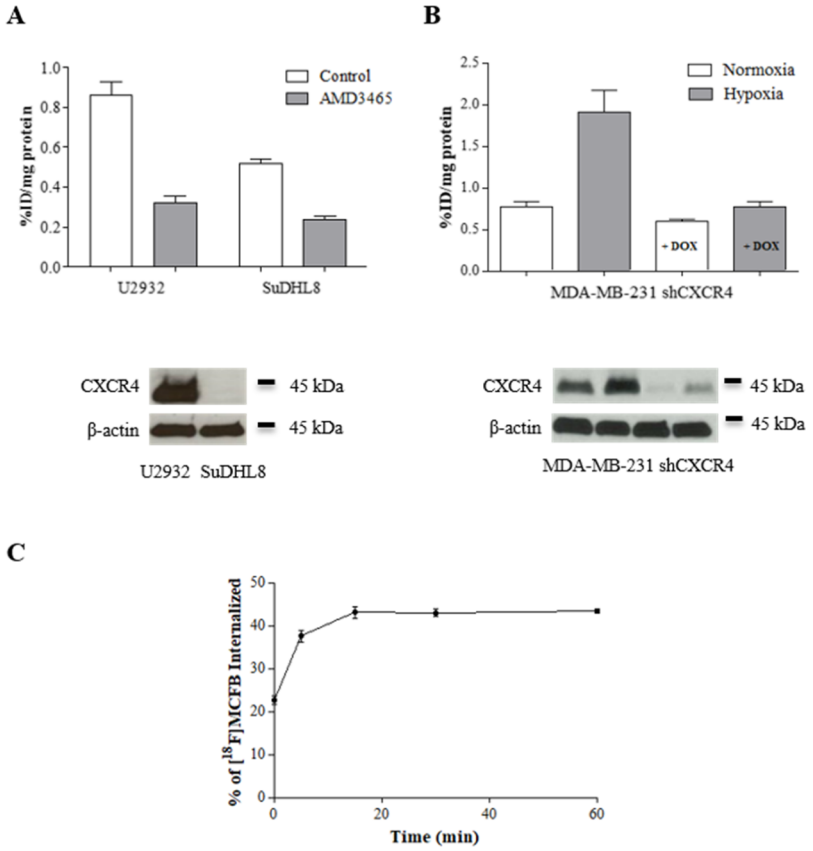

Figure 2. *In vitro* characterization of [^{18}F]MCFB. (A) Uptake of [^{18}F]MCFB normalized to cellular protein in U2932 and SuDHL8 cell lines, with or without blocking with AMD3465 (500 μM for 5 min). (B) Effect of CXCR4 knockdown on [^{18}F]MCFB radioactive uptake. MDA-MB-231 cells transduced with a doxycycline-inducible CXCR4-targeted (shCXCR4) short hairpin RNA construct were incubated under normoxia or hypoxia (<1% O_2 for 16 h) in the presence or absence of doxycycline (0.5 mg/mL for 24 h). Typical western blots of the CXCR4 expression (and β-actin as loading control) in U2932, SuDHL8, and MDA-MB-231 shCXCR4 cell lines are shown below. (C) Internalization of [^{18}F]MCFB in the MDA-MB-231 cell line. All data are mean ± SEM, n = 6.

Information Figure S2). The 50% inhibitory values (IC_{50}) for [^{19}F]MCFB and AMD3465 were 111.3 ± 4.0 and 89.8 ± 3.5 nM, respectively.

For *in vitro* binding studies, we used a highly expressing native CXCR4 B-cell lymphoma cell line, U2932, and compared it against another B-cell lymphoma cell line with lower CXCR4 expression, SuDHL8.[35] The [^{18}F]MCFB uptake was higher in the U2932 cell line (0.86 ± 0.15% ID/mg) than in SuDHL8 (0.52 ± 0.05% ID/mg), and coincubation with AMD3465 resulted in partial inhibition of tracer binding (63% for U2932 and 55% for SuDHL8). The difference in the tracer uptake between cell lines was smaller than the variation of the CXCR4 protein expression (96% difference of CXCR4/β-actin) (Figure 2A), and together with the partial blocking of tracer uptake after AMD3465 treatment, suggests some level of nonspecific binding.

Specific uptake of [^{18}F]MCFB was further confirmed by the use of isogenic MDA-MB-231 cells transduced with a doxycycline-inducible CXCR4-targeted shRNA (shCXCR4). Tracer accumulation was 2-fold higher in hypoxia-induced cells compared to normoxic conditions, in accordance with the higher CXCR4 expression (Figure 2B). Hypoxia induction was confirmed by HIF-1α expression (Supporting Information Figure S3). Receptor knockdown in the MDA-MB-231 shCXCR4 cell line by treatment with doxycycline resulted in a reduced tracer uptake, again demonstrating [^{18}F]MCFB sensitivity for the CXCR4 expression. In the control MDA-MB-231 shSC cell line, the cellular uptake of [^{18}F]MCFB was unperturbed by the doxycycline treatment, as expected (Supporting Information Figure S4). To determine the uptake mechanism, we incubated MDA-MB-231 cells with [^{18}F]MCFB at 4 °C, subsequently transitioning them to 37 °C. [^{18}F]MCFB was rapidly internalized, with the internal fraction reaching 40% of the total uptake within the first 15 min (Figure 2C). Indeed, at 37 °C, the internalized fraction was 9.8 ± 0.9% ID/mg, whereas at 4 °C, only 2.9 ± 0.3% ID/mg was found intracellularly (Supporting Information Figure S5), pointing to the role of internalization as part of the tracer uptake mechanism.

PET Imaging. Subsequently, we investigated tracer accumulation in mice bearing U2932 and SuDHL8 tumors, together with a nontransgenic variant of MDA-MB-231. Representative PET images show a high [^{18}F]MCFB accumulation in the tumor models at 60 min post radioligand injection (Figure 3A). The uptake was 2-fold higher in U2932 (T/WB ratio 4 ± 0.8) than in SuDHL8 (T/WB ratio 2.1 ± 0.3) and MDA-MB-231 (T/WB ratio 1.6 ± 0.1) (Figure 3B). Interestingly, the signal uptake (U2932 > SuDHL8 > MDA-MB-231) was not in accordance with the expression of CXCR4 (U2932 > MDA-MB-231 > SuDHL8).

This mismatch may be due to the central necrotic areas identified in the MDA-MB-231 tumors (Figure 3C). This phenotype has been described for this tumor model,[36] and the compromised vasculature can significantly reduce tracer

DOI: 10.1021/acs.molpharmaceut.9b00069
Mol. Pharmaceutics 2019, 16, 2106−2117

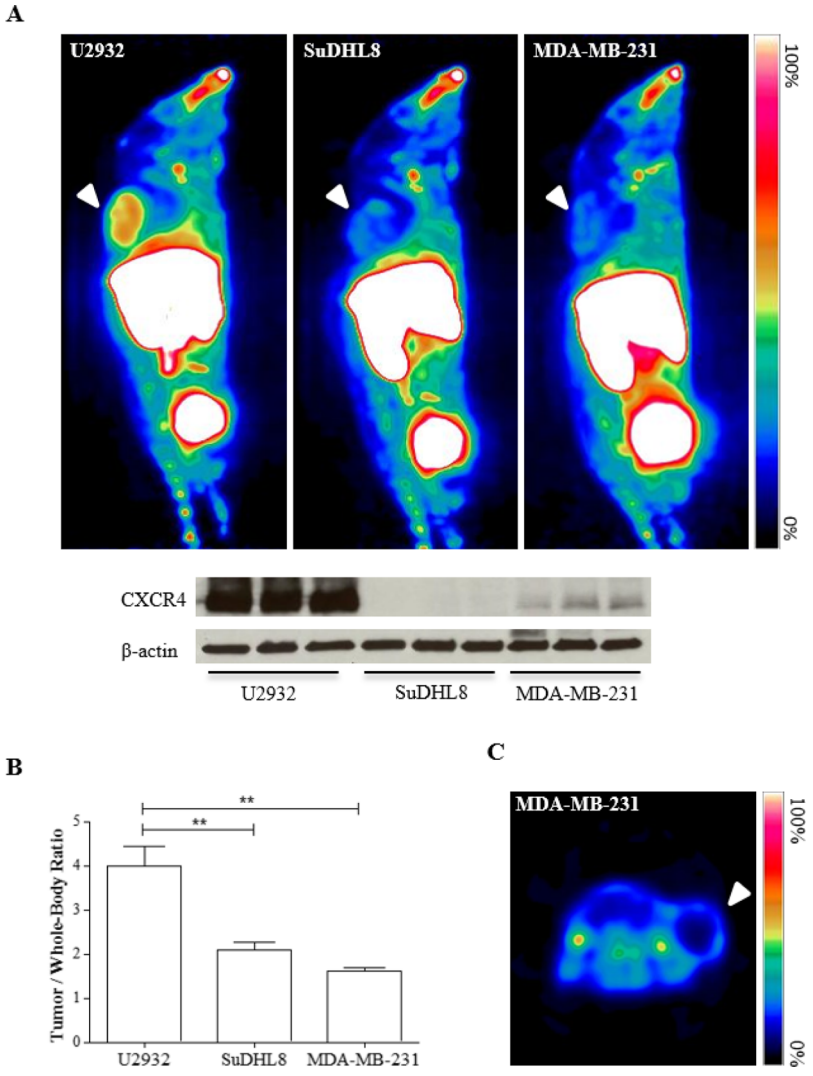

Figure 3. [^{18}F]MCFB discriminates differential CXCR4 expression *in vivo*. (A) Representative sagittal [^{18}F]MCFB-PET images derived from summed 60 min dynamic scans in U2932, SuDHL8, and MDA-MB-231 xenograft-bearing mice. CXCR4 expression in excised tumors was determined by western blot (results shown for three independent samples per tumor model). (B) Quantification of [^{18}F]MCFB uptake in the different tumor models by region of interest analysis normalized to whole-body radioactivity. Data are mean ± SEM, $n = 4$. (C) Representative axial [^{18}F]MCFB-PET image of a MDA-MB-231 xenograft-bearing mouse where necrosis is visible. White arrows indicate tumors.

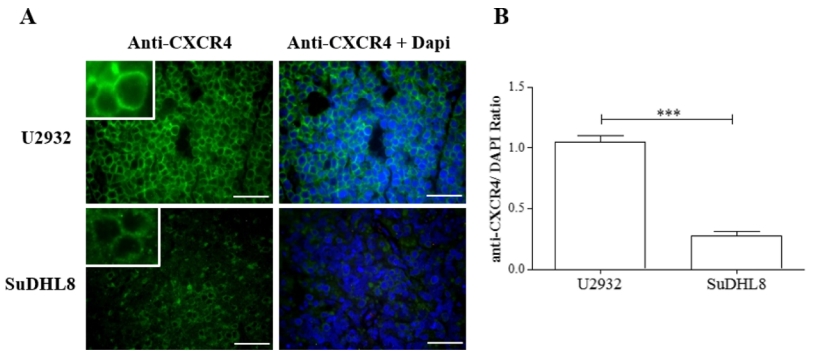

Figure 4. (A) Representative images of excised tumor tissues stained by immunofluorescence for CXCR4 (green) and DAPI (blue). (B) Quantification of the CXCR4-fluorescence intensity normalized to DAPI.

delivery not only to the necrotic core but also to the surrounding tissue. Thus, receptor binding in the whole tumor is likely to be affected, hindering differences in uptake between treatment groups, as was evident in our work. A high tracer uptake was also seen in the liver, bladder, and snout region.

Immunofluorescent staining of the excised tumors showed expression of CXCR4 in both cell lymphoma lines (Figure 4A), although significantly higher in U2932 compared to SuDHL8 ($p < 0.001$) (Figure 4B).

DOI: 10.1021/acs.molpharmaceut.9b00069
Mol. Pharmaceutics 2019, 16, 2106−2117

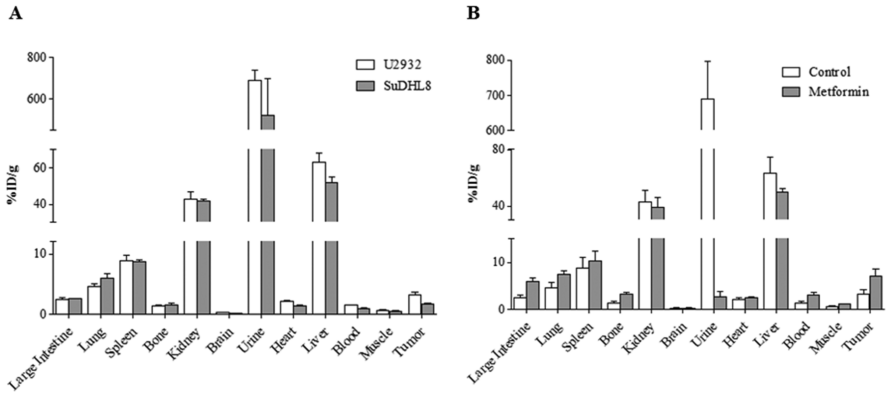

Figure 5. Biodistribution of [^{18}F]MCFB. (A) Mice bearing U2932 and SuDHL8 xenografts and (B) mice bearing U2932 treated with 50 mg/kg of metformin for 30 min were injected with 1.48 MBq of [^{18}F]MCFB, and tissues were excised 60 min after injection. Radioactivity in the tissues was counted and is expressed as a fraction of the injected dose normalized to the tissue weight. Data are mean ± SEM, n = 4.

[^{18}F]MCFB Biodistribution. Biodistribution was carried out in U2932 and SuDHL8 tumor-bearing mice 60 min after injection of [^{18}F]MCFB (Figure 5A). Tumor uptake was 3.3 ± 0.91% ID/g for U2932 tumors and 1.81 ± 0.04% ID/g for SuDHL8 tumors. The low levels of bone uptake for both SuDHL8- and U2932-bearing mice (1.6 ± 0.3 and 1.4 ± 0.2% ID/g, respectively) suggest that tracer defluorination did not ensue upon intravenous injection, and renal elimination occurred as indicated by the high tracer localization in kidneys (42.1 ± 1.8 and 43.1 ± 7.3% ID/g, respectively) and urine (521.7 ± 178.5 and 688.8 ± 50.4% ID/g, respectively). High [^{18}F]MCFB accumulation in the liver was also seen (51.9 ± 2.9% ID/g for SuDHL8- and 63.0 ± 4.9% ID/g for U2932-bearing mice).

Radio-chromatographic analysis of plasma and liver extracts obtained at 15 or 60 min after [^{18}F]MCFB injection showed only the parent compound indicating good *in vivo* metabolic stability (Supporting Information Figure S6), suggesting that the high liver uptake was unlikely due to metabolism. Similar to AMD3465, [^{18}F]MCFB has a positive charge at physiological pH. We hypothesized that polyspecific transporters, such as OCT1, OCT2, and OCT3, may be involved in the transport of the tracer into the metabolic organs. To test this hypothesis, we treated U2932 tumor-bearing mice with 50 mg/kg of metformin, an oral insulin-sensitizing drug that is a substrate for OCT1, OCT2, and OCT3, and imaged the mice with [^{18}F]MCFB (Figure 5B and Supporting Information Figure S7). Biodistribution studies showed a marked decrease in the urinary excretion of [^{18}F]MCFB after metformin treatment (688.8 ± 50.4% to 2.8 ± 0.4% ID/mg) and a moderate decrease in the kidneys and liver; all other organs showed small increases in the [^{18}F]MCFB uptake.

DISCUSSION

We report the development of the ^{18}F cyclam-based radioligand, [^{18}F]MCFB, designed for sensitive detection of CXCR4. Several PET-dedicated tracers have been developed for the imaging of CXCR4 by exploiting the modifications of therapeutically relevant antagonists to accommodate different radioisotopes. Cyclam-based tracers, such as AMD3100 and AMD3465, have shown promising characteristics for CXCR4 imaging; however, they have also been plagued with high hepatic accumulation. Given that CXCR4 is expressed in the liver, some degree of specific liver uptake is expected. Most strategies employ ^{64}Cu for the radiolabeling of cyclams, whose structures accommodate metals without the need of a chelator. However, ^{64}Cu is known to undergo transchelation[37] and could contribute to nonspecific uptake in the liver. This is supported by a previous work with the ^{18}F-radiolabeled T140 peptide that showed significantly lower accumulation in the liver compared to its analogous radiometal chelates.[7,8] From the foregoing discussion, we designed a new monocyclam ligand to incorporate an ^{18}F radiolabel to exploit the physical properties of ^{18}F and potentially improve the *in vivo* biodistribution. This work describes the synthesis and preclinical evaluation of the resulting tracer, [^{18}F]MCFB.

Mutational mapping and molecular modelling showed that the amino groups of these cyclams are important in binding to CXCR4 via electrostatic interactions between the positively charged nitrogens and the negatively charged carboxylates present within the CXCR4 protein. [^{18}F]MCFB was designed based on the AMD3465 structure; the minimum number of nitrogen atoms required to achieve sufficient interaction with the CXCR4-active binding site through hydrogen bonding was preserved.[38] Thus, interaction with CXCR4 was not compromised: the IC_{50} of [^{19}F]MCFB (111.3 nM) for CXCR4 was comparable to that of AMD3465 (89.8 nM).

Our results showed that the cellular uptake of [^{18}F]MCFB was sensitive to modulation of the CXCR4 expression within the same cellular background: knockdown of CXCR4 with shRNA decreased the [^{18}F]MCFB uptake, whereas hypoxia increased the radioligand uptake, consistent with differences in the CXCR4 expression. Furthermore, the tracer was able to differentiate between two cell lines, U2932 and SuDHL8, with different CXCR4 expressions *in vitro*, and the uptake was inhibited in the presence of AMD3465. The observation that the uptake in U2932 and SuDHL8 did not entirely reflect the difference in the CXCR4 expression indicates a degree of nonspecific binding of the radiotracer.

Consistent with its negative log $D_{octanol/PBS}$, studies in MDA-MB-231 showed that [^{18}F]MCFB was rapidly internalized and remained inside the cell, in a similar fashion to [^{64}Cu]-AMD3465[19] and *N*-[^{11}C]methyl-AMD3465.[18] We have shown that CXCR4 is also expressed in the intracellular compartments of MDA-MB-231 (Supporting Information Figure S8); thus, radiotracer binding to cytosolic proteins, following possible release from internalized CXCR4 in cells, for instance, could potentially result in retention and higher signal-to-noise ratio. It therefore appears that the nonspecific binding of [^{18}F]MCFB to cells does not result from defective internal-

DOI: 10.1021/acs.molpharmaceut.9b00069
Mol. Pharmaceutics 2019, 16, 2106−2117

ization. Furthermore, the surface expression of the analogous receptor that shares binding to SDF-1, CXCR7, occurred at low but equivalent levels in both U2932 and SuDHL8 cells (Supporting Information Figure S9) and thus does not explain the nonspecific binding.

On the basis of the 60-min dynamic PET data, we performed quantification of [^{18}F]MCFB *in vivo* at 40−60 min post tracer injection. [^{18}F]MCFB showed sufficiently high tumor-to-background localization to permit tumor detection. As with the *in vitro* studies, the difference in the tracer uptake was disproportionate to differences in the CXCR4 protein expression between U2932 and SuDHL8 by western blot *in vivo*; this could be the result of limitations of the technique, as it can only provide relative measurements. Indeed, immunofluorescence staining of excised specimens showed a low but detectable CXCR4 expression in the SuDHL8 tumors, in accordance with the existing literature.[35]

In vivo biodistribution of [^{18}F]MCFB showed a high uptake in organs such as liver, lung, and spleen, with high levels of CXCR4, similar to the profile reported for CXCR4-based PET tracers.[18,19] The accumulation of [^{18}F]MCFB in the CXCR4-expressing tumor tissue derived from naturally occurring models was only modest (3.3 ± 0.91 and 1.81 ± 0.04% ID/g for U2932 and SuDHL8, respectively) but similar to the uptake of [^{18}F]RPS-544 in a CXCR4-overexpressing model (3.4 ± 1.2% ID/g in PC3-CXCR4 tumors).[24] Although it would be reasonable to expect more uptake of the radioligand in transgenic cells than in naturally derived cells, head-to-head comparison of [^{18}F]MCFB and previously reported radiolabeled cyclams is challenging owing to the use of models with vastly different CXCR4 profiles.

High radioactivity accumulation in the urine and kidneys indicate that elimination of [^{18}F]MCFB occurred via the urinary system. The uptake of [^{18}F]MCFB in the liver was similar to other AMD3465-based imaging agents (liver-to-muscle ratio of 74, 86, and 150 for [^{18}F]MCFB, [^{64}Cu]-AMD3465, and *N*-[^{11}C]methyl-AMD3465, respectively). The clearance of [^{18}F]MCFB differed from [^{18}F]RPS-544, which showed a high uptake in small and large intestines; the excretion of [^{18}F]MCFB was more similar to nonfluorine-containing cyclam-based radioligands reported in the literature.

Metabolite analysis of [^{18}F]MCFB from the mouse plasma, urine, and liver (tissues excised 1 h p.i.) by radio-HPLC showed only the presence of the parent compound (Supporting Information Figure S6). However, it should be noted that the extraction efficiency was not measured, and thus any insoluble metabolites or adducts formed between the parent and liver would not have been detected by the method used. Bone uptake was found to be low suggesting that defluorination was negligible or absent; this was expected as defluorination of fluorinated arenes is uncommon.

The liver plays an essential role in removing drugs or toxins from circulation in the human body as well as in the clearance of various endogenous compounds.[39] At physiological pH, several compounds are positively charged, thus requiring transport proteins to facilitate crossing the plasma membrane into the hepatocytes. OCTs mediate the uptake of a wide variety of these compounds; OCT1, expressed primarily in the liver, is particularly important in the hepatic elimination of numerous small molecules.[40] At physiological pH, both AMD3100 and AMD3465 have a positive charge, owing to the charged nitrogens in the cyclam moieties.[41] Similarly, [^{18}F]MCFB has a positive charge, which led us to hypothesize that it may be a substrate for OCTs. Metformin is a substrate for OCT1, which has been reported as the primary hepatic transporter for this drug.[42] Predosing with metformin led to a small decrease in the [^{18}F]MCFB uptake in the liver, which, together with the increased radioactivity in the blood, suggests some level of competitive inhibition of OCT1 (and perhaps OCT3) in this organ. A marked decrease in the urinary excretion of [^{18}F]MCFB suggests involvement of these polyspecific transporters in the renal elimination of the tracer. Interestingly, the decrease of [^{18}F]MCFB uptake in urine was not reflected in the kidney. OCT2 is important for the renal clearance of metformin and its subsequent excretion into urine.[43] Given the rapid clearance of metformin, we speculate that competitive inhibition of [^{18}F]MCFB kinetics by metformin is only transient, with partial restoration of OCT2 over time such that by 60 min—the time point in biodistribution studies—the localization of [^{18}F]MCFB in the kidneys of metformin-treated mice is not significantly different from that of metformin-naïve mice. In contrast, urine radioactivity reflects the cumulative elimination of radioactivity over the entire 60 min period and more accurately reflects the kidney function, compared to kidney [^{18}F]MCFB-derived radioactivity at any one time point. This is consistent with previously reported results, whereby [11C]-labeled metformin was coinjected with unlabeled metformin; the authors showed decreased urinary clearance in the presence of unlabeled metformin, in agreement with a pharmacokinetic profile showing higher kidney radioactivity at very early time points and becoming similar at 60 min, that is, higher kidney exposure in the untreated tumors concordant with higher urine levels.[44]

However, this work is only a preliminary study, and the extent of transport inhibition would need to be assessed with a range of metformin concentrations.

Further work in well-defined CXCR4 nonexpressing cells (e.g., via CRISPR) is also required to verify if various OCTs contribute to the nonspecific binding of [^{18}F]MCFB in tumor cells.

Overall, these data suggest that the high liver uptake seen with cyclam-based tracers is likely to be influenced by a variety of mechanisms; besides the CXCR4-mediated uptake and transchelation of radiometals (not relevant to ^{11}C or ^{18}F candidates), the high overall positive charge [^{18}F]MCFB required for the CXCR4 receptor interaction may also contribute to nonspecific interactions, as recently described by others for similar cyclams.[45] Of note, this is not due to lipophilicity as the measured log $D_{\text{octanol/PBS}}$ was in the negative range—which also precludes it from passing the blood brain barrier (BBB). Therefore, the radioligand appears unsuitable for imaging both brain (without a compromised BBB) and liver lesions but adequate for use in nonabdominal anatomical locations, although more work would be necessary to optimize the pharmacokinetics for use in abdominal regions *in vivo*.

CONCLUSIONS

We report the design, synthesis, and biological testing of a novel and promising ^{18}F-radiolabeled cyclam, [^{18}F]MCFB, for PET imaging of the CXCR4 expression. [^{18}F]MCFB showed a CXCR4-dependent specific and sensitive uptake, though some nonspecific binding was also seen. *In vivo* imaging demonstrated that this tracer is capable of tumor detection and CXCR4 characterization in models with a naturally occurring receptor expression. Elevated hepatic uptake complicates the detection of liver metastases; but it is in conformity with other

DOI: 10.1021/acs.molpharmaceut.9b00069
Mol. Pharmaceutics 2019, 16, 2106−2117

cyclam-based PET agents. Nonetheless, [^{18}F]MCFB showed potential as a CXCR4-targeting tracer.

■ ASSOCIATED CONTENT

Supporting Information

The Supporting Information is available free of charge on the ACS Publications website at DOI: 10.1021/acs.molpharmaceut.9b00069.

Materials and methods for immunofluorescence and flow cytometry; affinity of [^{19}F]MCFB for the CXCR4 receptor; confirmation of hypoxia induction by HIF-1α protein expression analysis;*in vitro* uptake of [^{18}F]MCFB in the control cell line MDA-MB-231 shSC; *in vivo* stability of [^{18}F]MCFB in the mouse plasma, urine, and liver; subcellular localization of CXCR4; and expression of CXCR7 in U2932 and SuDHL8 cell lines determined by flow cytometry (PDF)

■ AUTHOR INFORMATION

Corresponding Author

*E-mail: e.aboagye@imperial.ac.uk. Phone: +44 (0)20 3313 3759.

ORCID

Marta Braga: 0000-0002-2673-776X

Author Contributions

†D.B. and M.B. contributed equally to this work.

Notes

The authors declare no competing financial interest.

■ ACKNOWLEDGMENTS

This work was funded by the Cancer Research UK-Engineering and Physical Sciences Research Council [in association with the Medical Research Council and Department of Health (England)] grant C2536/A10337 and the Cancer Research UK grant C2536/A16584. E.O.A. acknowledges support from the Imperial College NIHR Biomedical Research Centre award (WSCC_P62585), the Medical Research Council grant (MC-A652-5PY80), and the Experimental Cancer Medicine Centres grant (C37/A7283). We thank Dr. Louis Allott for all his help and support throughout the writing of this manuscript.

■ REFERENCES

(1) Teicher, B. A.; Fricker, S. P. CXCL12 (SDF-1)/CXCR4 pathway in cancer. *Clin. Cancer Res.* **2010**, *16*, 2927−2931.

(2) Domanska, U. M.; Kruizinga, R. C.; Nagengast, W. B.; et al. A review on CXCR4/CXCL12 axis in oncology: No place to hide. *Eur. J. Cancer* **2013**, *49*, 219−230.

(3) Müller, A.; Homey, B.; Soto, H.; et al. Involvement of chemokine receptors in breast cancer metastasis. *Nature* **2001**, *410*, 50−56.

(4) Burger, J. A.; Kipps, T. J. CXCR4: a key receptor in the crosstalk between tumor cells and their microenvironment. *Blood* **2006**, *107*, 1761−1767.

(5) Kopp, H.-G.; Ramos, C. A.; Rafii, S. Contribution of endothelial progenitors and proangiogenic hematopoietic cells to vascularization of tumor and ischemic tissue. *Curr. Opin. Hematol.* **2006**, *13*, 175−181.

(6) Shi, J.; Wei, Y.; Xia, J.; et al. CXCL12−CXCR4 contributes to the implication of bone marrow in cancer metastasis. *Future Oncol.* **2014**, *10*, 749−759.

(7) Jacobson, O.; Weiss, I. D.; Kiesewetter, D. O.; Farber, J. M.; Chen, X. PET of tumor CXCR4 expression with 4-18F-T140. *J. Nucl. Med.* **2010**, *51*, 1796−1804.

(8) Jacobson, O.; Weiss, I. D.; Szajek, L. P.; et al. PET imaging of CXCR4 using copper-64 labeled peptide antagonist. *Theranostics* **2011**, *1*, 251−262.

(9) Jacobson, O.; Weiss, I. D.; Szajek, L. P.; et al. Improvement of CXCR4 tracer specificity for PET imaging. *J. Controlled Release* **2012**, *157*, 216−223.

(10) Gourni, E.; Demmer, O.; Schottelius, M.; et al. PET of CXCR4 expression by a (68)Ga-labeled highly specific targeted contrast agent. *J. Nucl. Med.* **2011**, *52*, 1803−1810.

(11) Demmer, O.; Gourni, E.; Schumacher, U.; Kessler, H.; Wester, H.-J. PET Imaging of CXCR4 Receptors in Cancer by a New Optimized Ligand. *ChemMedChem* **2011**, *6*, 1789−1791.

(12) Debnath, B.; Xu, S.; Grande, F.; Garofalo, A.; Neamati, N. Small Molecule Inhibitors of CXCR4. *Theranostics* **2013**, *3*, 47−75.

(13) Jacobson, O.; Weiss, I. D.; Szajek, L.; Farber, J. M.; Kiesewetter, D. O. 64Cu-AMD3100—A novel imaging agent for targeting chemokine receptor CXCR4. *Bioorg. Med. Chem.* **2009**, *17*, 1486−1493.

(14) Nimmagadda, S.; Pullambhatla, M.; Stone, K.; Green, G.; Bhujwalla, Z. M.; Pomper, M. G. Molecular imaging of CXCR4 receptor expression in human cancer xenografts with [64Cu]-AMD3100 positron emission tomography. *Cancer Res.* **2010**, *70*, 3935−3944.

(15) De Silva, R. A.; Peyre, K.; Pullambhatla, M.; Fox, J. J.; Pomper, M. G.; Nimmagadda, S. Imaging CXCR4 expression in human cancer xenografts: evaluation of monocyclam 64Cu-AMD3465. *J. Nucl. Med.* **2011**, *52*, 986−993.

(16) Woodard, L. E.; De Silva, R. A.; Behnam Azad, B.; et al. Bridged cyclams as imaging agents for chemokine receptor 4 (CXCR4). *Nucl. Med. Biol.* **2014**, *41*, 552−561.

(17) Poty, S.; Gourni, E.; Désogère, P.; et al. AMD3100: A Versatile Platform for CXCR4 Targeting 68Ga-Based Radiopharmaceuticals. *Bioconjugate Chem.* **2016**, *27*, 752−761.

(18) Hartimath, S. V.; van Waarde, A.; Dierckx, R. A. J. O.; de Vries, E. F. J. Evaluation of N-[(11)C]methyl-AMD3465 as a PET tracer for imaging of CXCR4 receptor expression in a C6 glioma tumor model. *Mol. Pharm.* **2014**, *11*, 3810−3817.

(19) De Silva, R. A.; Peyre, K.; Pullambhatla, M.; Fox, J. J.; Pomper, M. G.; Nimmagadda, S. Imaging CXCR4 Expression in Human Cancer Xenografts: Evaluation of Monocyclam 64Cu-AMD3465. *J. Nucl. Med.* **2011**, *52*, 986−993.

(20) Shibuta, K.; Mori, M.; Shimoda, K.; Inoue, H.; Mitra, P.; Barnard, G. F. Regional expression of CXCL12/CXCR4 in liver and hepatocellular carcinoma and cell-cycle variation during in vitro differentiation. *Jpn. J. Cancer Res.* **2002**, *93*, 789−797.

(21) Liang, Z.; Zhan, W.; Zhu, A.; et al. Development of a Unique Small Molecule Modulator of CXCR4. *PLoS One* **2012**, *7*, No. e34038.

(22) Demoin, D. W.; Shindo, M.; Zhang, H.; et al. Synthesis and evaluation of an 18F-labeled pyrimidine-pyridine amine for targeting CXCR4 receptors in gliomas. *Nucl. Med. Biol.* **2016**, *43*, 606−611.

(23) Poty, S.; Désogère, P.; Goze, C.; et al. New AMD3100 derivatives for CXCR4 chemokine receptor targeted molecular imaging studies: synthesis, anti-HIV-1 evaluation and binding affinities. *Dalton Trans.* **2015**, *44*, 5004−5016.

(24) Amor-Coarasa, A.; Kelly, J.; Ponnala, S.; et al. [18F]RPS-544: A PET tracer for imaging the chemokine receptor CXCR4. *Nucl. Med. Biol.* **2018**, *60*, 37−44.

(25) Dolle, F. Fluorine-18-labelled fluoropyridines: advances in radiopharmaceutical design. *Curr. Pharm. Des.* **2005**, *11*, 3221−3235.

(26) Wilson, A. A.; Dannals, R. F.; Ravert, H. T.; Wagner, H. N. Reductive amination of [18F]fluorobenzaldehydes: Radiosyntheses of [2-18F]- and [4-18F]fluorodexetimides. *J. Labelled Compd. Radiopharm.* **1990**, *28*, 1189−1199.

(27) Chang, Y. S.; Jeong, J. M.; Lee, Y.-S.; et al. Preparation of 18F-human serum albumin: A simple and efficient protein labeling method with 18F using a hydrazone-formation method. *Bioconjugate Chem.* **2005**, *16*, 1329−1333.

DOI: 10.1021/acs.molpharmaceut.9b00069
Mol. Pharmaceutics 2019, 16, 2106−2117

(28) George, G. P. C.; Stevens, E.; Åberg, O.; et al. Preclinical evaluation of a CXCR4-specific (68)Ga-labelled TN14003 derivative for cancer PET imaging. *Bioorg. Med. Chem.* **2014**, *22*, 796−803.
(29) Workman, P.; Aboagye, E. O.; Balkwill, F.; et al. Guidelines for the welfare and use of animals in cancer research. *Br. J. Cancer* **2010**, *102*, 1555−1577.
(30) Nguyen, Q.-D.; Smith, G.; Glaser, M.; Perumal, M.; Arstad, E.; Aboagye, E. O. Positron emission tomography imaging of drug-induced tumor apoptosis with a caspase-3/7 specific [18F]-labeled isatin sulfonamide. *Proc. Natl. Acad. Sci. U.S.A.* **2009**, *106*, 16375−16380.
(31) Witney, T. H.; Pisaneschi, F.; Alam, I. S.; et al. Preclinical evaluation of 3-18F-fluoro-2,2-dimethylpropionic acid as an imaging agent for tumor detection. *J. Nucl. Med.* **2014**, *55*, 1506−1512.
(32) Evans, H. L.; Nguyen, Q.-D.; Carroll, L. S.; et al. A bioorthogonal 68Ga-labelling strategy for rapid in vivo imaging. *Chem. Commun.* **2014**, *50*, 9557−9560.
(33) Wilcock, C.; Bailey, C. J. Accumulation of metformin by tissues of the normal and diabetic mouse. *Xenobiotica* **1994**, *24*, 49−57.
(34) Yang, W.; Giandomenico, C. M.; Sartori, M.; Moore, D. A. Facile N-1 protection of cyclam, cyclen and 1,4,7-triazacyclononane. *Tetrahedron Lett.* **2003**, *44*, 2481−2483.
(35) Wester, H. J.; Keller, U.; Schottelius, M.; et al. Disclosing the CXCR4 expression in lymphoproliferative diseases by targeted molecular imaging. *Theranostics* **2015**, *5*, 618−630.
(36) Nofiele, J. T.; Cheng, H.-L. M.; Hart, G.; Shilkaitis, A.; Gupta, T. D. Establishment of a Lung Metastatic Breast Tumor Xenograft Model in Nude Rats. *PLoS One* **2014**, *9*, No. e97950.
(37) Rogers, B. E.; Anderson, C. J.; Connett, J. M.; et al. Comparison of Four Bifunctional Chelates for Radiolabeling Monoclonal Antibodies with Copper Radioisotopes: Biodistribution and Metabolism. *Bioconjugate Chem.* **1996**, *7*, 511.
(38) Hatse, S.; Princen, K.; Clercq, E. D.; et al. AMD3465, a monomacrocyclic CXCR4 antagonist and potent HIV entry inhibitor. *Biochemical Pharmacology* **2005**, *70*, 752.
(39) Coleman, M. D. *Human Drug Metabolism: An Introduction*; Wiley-Blackwell, 2010.
(40) Boxberger, K. H.; Hagenbuch, B.; Lampe, J. N. Common drugs inhibit human organic cation transporter 1 (OCT1)-mediated neurotransmitter uptake. *Drug Metab. Dispos.* **2014**, *42*, 990−995.
(41) De Clercq, E. The bicyclam AMD3100 story. *Nat. Rev. Drug Discovery* **2003**, *2*, 581−587.
(42) Chen, L.; Shu, Y.; Liang, X.; et al. OCT1 is a high-capacity thiamine transporter that regulates hepatic steatosis and is a target of metformin. *Proc. Natl. Acad. Sci. U.S.A.* **2014**, *111*, 9983−9988.
(43) Chen, Y.; Li, S.; Brown, C.; et al. Effect of genetic variation in the organic cation transporter 2 on the renal elimination of metformin. *Pharmacogenet. Genomics* **2009**, *19*, 497−504.
(44) Jakobsen, S.; Busk, M.; Jensen, J. B.; et al. A PET Tracer For Renal Organic Cation Transporters, 11 C-metformin: Radiosynthesis and Preclinical Proof-of-Concept Studies. *J. Nucl. Med.* **2016**, *57*, 615.
(45) Frindel, M.; Camus, N.; Rauscher, A.; et al. Radiolabeling of HTE1PA: A new monopicolinate cyclam derivative for Cu-64 phenotypic imaging. In vitro and in vivo stability studies in mice. *Nucl. Med. Biol.* **2014**, *41*, e49−e57.

DOI: 10.1021/acs.molpharmaceut.9b00069
Mol. Pharmaceutics 2019, 16, 2106−2117